

## Chapman University Chapman University Digital Commons

---

Mathematics, Physics, and Computer Science  
Faculty Articles and Research

Science and Technology Faculty Articles and  
Research

---


1983

# The High-Energy Spectrum of Hot Accretion Disks

J. A. Eilek  
*New Mexico Tech*

Menas Kafatos  
*Chapman University*, [kafatos@chapman.edu](mailto:kafatos@chapman.edu)

Follow this and additional works at: [http://digitalcommons.chapman.edu/scs\\_articles](http://digitalcommons.chapman.edu/scs_articles)

 Part of the [External Galaxies Commons](#), and the [Stars, Interstellar Medium and the Galaxy Commons](#)

---

### Recommended Citation

Eilek, J.A., Kafatos, M. (1983) The High-Energy Spectrum of Hot Accretion Disks, *Astrophysical Journal*, 271: 804-819. doi: 10.1086/161246

This Article is brought to you for free and open access by the Science and Technology Faculty Articles and Research at Chapman University Digital Commons. It has been accepted for inclusion in Mathematics, Physics, and Computer Science Faculty Articles and Research by an authorized administrator of Chapman University Digital Commons. For more information, please contact [laughtin@chapman.edu](mailto:laughtin@chapman.edu).

---

# The High-Energy Spectrum of Hot Accretion Disks

## **Comments**

This article was originally published in *Astrophysical Journal*, volume 271, in 1983. DOI: [10.1086/161246](https://doi.org/10.1086/161246)

## **Copyright**

IOP Publishing

## THE HIGH-ENERGY SPECTRUM OF HOT ACCRETION DISKS

JEAN A. EILEK

National Radio Astronomy Observatory,<sup>1</sup> Charlottesville, VA; and Physics Department, New Mexico Tech

AND

MINAS KAFATOS

Physics Department, George Mason University  
 Received 1982 August 20; accepted 1983 January 27

### ABSTRACT

A hot, two-temperature accretion disk can be a strong  $\gamma$ -ray and relativistic particle source. This occurs when the accretion rate is high enough— $\dot{M}/M \geq 3 \times 10^{-9} \alpha \text{ yr}^{-1}$  for a canonical Kerr black hole—due to the high ion temperature in the inner disk. We present detailed photon and particle spectra for specific disk models. The predicted  $\gamma$ -ray flux is as high as 10% of the bolometric luminosity in sub-Eddington models. Most of the  $\gamma$ -radiation is continuous, due to the  $\pi^0$  decay, emitted around 100 MeV but degraded to a few MeV in optically thick models. Spectral lines, due to positron annihilation or to excited nuclei, provide only a small amount of the primary  $\gamma$ -ray luminosity. The energy flux in  $\sim 35$  MeV pairs is comparable to the  $\gamma$ -ray luminosity; Penrose effects provide a smaller number of  $\sim 1$  GeV pairs.

Applications of the model both to galactic and extragalactic sources are discussed. Both the galactic center  $\gamma$ -ray source and the extragalactic  $\gamma$ -ray background (if it is due to discrete sources) may be due to this type of model.

*Subject headings:* black holes — galaxies: nuclei — gamma rays: general — particle acceleration — radiation mechanisms — stars: accretion

### I. INTRODUCTION

Hot optically thin accretion disks appear to be successful as models for galactic X-ray sources, such as Cyg X-1. It also may be that these hot disks exist around massive black holes in active galactic nuclei. If the electrons have a temperature  $T_e \geq 10^8$  K and the plasma is characterized by a Comptonization parameter  $y = (4kT_e/m_e c^2) \max(\tau_{es}, \tau_{es}^2) \approx 1$ , then unsaturated Compton cooling using an abundant soft photon source will control the electron temperature and also produce an X-ray spectrum with photon energies up to  $h\nu_{\max} \approx kT_e$ .

Two detailed hot disk models have been proposed. The thermal state of the plasma in each one depends on the strength of the thermal coupling between electrons and ions in the hot plasma. Shapiro, Lightman, and Eardley (1976, SLE) assume that viscosity mainly heats the ions, and that only Coulomb interactions transfer energy between the ions and electrons. Strong radiative electron cooling then leads to  $T_i > T_e$ , and the “two-temperature” disk model. Liang and Price (1977) and Liang and Thompson (1979, LT) assume some unspecified coupling forces  $T_i = T_e$ , and suggest a single temperature corona sandwiching a cool, optically thick disk.

Both of these models appear able to explain the X-ray spectrum of active nuclei or of galactic sources. One important difference, however, has been pointed out by Eilek (1980, Paper I). She noted that the very high ion temperatures in the two-temperature disk can lead to pion production, which in turn leads to creation of  $\gamma$ -rays, relativistic particles, and neutrinos. This is useful in two ways. First, a strong  $\gamma$ -ray flux—at 1 to 100 MeV, depending on the disk parameters—is potentially observable and could be used as a discriminant between the two models. Second, if the  $T_i \gg T_e$  phase does exist, the high-energy quanta produced could be important astrophysically in active nuclei. The  $\gamma$ -ray spectra can be compared to the few observations of individual objects that we have so far, and also to the extragalactic  $\gamma$ -ray background which may be due to discrete sources such as quasars. The appearance of relativistic particles in an accretion disk is important for explaining the radio synchrotron sources, and possible self-Compton effects, in active nuclei. The neutrino flux is presently unobservable.

<sup>1</sup>The National Radio Astronomy Observatory is operated by Associated Universities, Incorporated, under contract with the National Science Foundation.

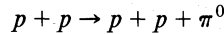
Because of the importance of any  $\gamma$ -rays and energetic particles from accretion disks—both as a discriminant between the two hot disk models, and as a possible source of energetic quanta from discrete sources as well as the  $\gamma$ -ray background—we expand on Paper I by calculating detailed disk models and the  $\gamma$ -ray and particle spectra arising from them. Our approach is to take a set of disk parameters, calculate the resulting disk model, and evaluate the spectrum it produces. Kafatos (1980) has taken a different approach. He assumes the  $\gamma$ -ray flux from active nuclei is due to a specific process—Penrose effects, which we discuss below—and derives constraints on disk models that allow this process to go.

As in Paper I, we assume a two-temperature disk in a Kerr metric (which includes the Schwarzschild case, of course). The important parameters turn out to be the angular momentum of the hole,  $a_*$ , the fractional accretion rate,  $\dot{M}/M$ , and two artificial model parameters, the Comptonization factor,  $y$ , and the viscosity factor,  $\alpha$ . We will show that for high (but sub-Eddington) values of  $\dot{M}/M$ , the  $\gamma$ -ray luminosity is as high as 10% of the bolometric luminosity; the energy flux in positrons and electrons is comparable. Both photons and particles are produced in a peak around 100 MeV (although the photons may be degraded due to optical depth effects). We will show that Penrose effects do occur but are not dominant. Since  $\dot{M}/M$  controls  $T_i$  and hence pion production, these results hold for galactic stellar sources as well as massive black holes in active galactic nuclei.

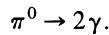
## II. PRODUCTION OF HIGH-ENERGY QUANTA IN A HOT ION GAS

### a) Determining the Spectrum

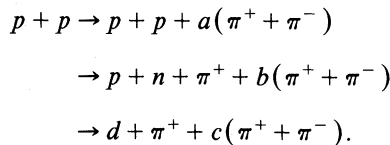
We want to determine in some detail the spectrum of hard photons and energetic particles due to pion reactions in a plasma with ion temperature  $\geq 10^{12}$  K. This requires looking at the kinematics of individual reactions. We consider neutral pions produced in



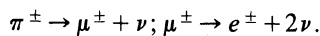
(single pion production is the most important mode below 1 GeV) and the subsequent decay,



Charged pions are produced, for proton energies below 1 GeV, in the reactions



The charged pion decays through a muon to an electron (a positron or negaton);



The average energy of a pion (of any charge) arising in a  $pp$  reaction can be written,

$$\bar{\gamma} = 1 + (\gamma_p - 1)^{3/4}. \quad (1)$$

This is a good representation of the data presented by Ramaty and Lingenfelter (1966) at energies above a few GeV. Perola, Scarsi, and Sironi (1967) give low-energy data on the spread of  $\gamma_\pi$  resulting from a given  $\gamma_p$ . Their data show that for  $\gamma_p < 2$ , the  $\gamma_\pi(\gamma_p)$  curve turns down, so that  $\bar{\gamma}_\pi \rightarrow 1$  as  $\gamma_p \rightarrow \gamma_{pT} = 1.37$ , the threshold ( $T_p = 290$  MeV). We shall write  $\bar{\gamma}_\pi = g(\gamma_p)$  generally, and in calculation use the representation (1) for its simplicity, while keeping in mind the slight error at low  $\gamma_p$ . The cross section for pion production can then be written

$$\sigma_\pi(\gamma_\pi, \gamma_p) = \Sigma_\pi(\gamma_p) \delta[\gamma_\pi - g(\gamma_p)], \quad (2)$$

where  $\Sigma_\pi(\gamma_p)$  gives the magnitude of the cross section for species  $\pi(\pi^+, \pi^0, \text{ or } \pi^-)$  (these are listed in Table 1).

TABLE I  
 PION PRODUCTION CROSS SECTIONS USED IN CALCULATION

$\pi^0$ : $\Sigma_{\pi^0}(\gamma_p) = 1.4 \times 10^{-26} (\gamma_p - 1)^{7.375} \text{ cm}^2$	$(\gamma_p < 2)$
$= 8.4 \times 10^{-27} \gamma_p^{0.75}$	$(\gamma_p > 2)$
$\pi^+$ : $\Sigma_{\pi^+}(\gamma_p) = 3.4 \times 10^{-26} (\gamma_p - 1)^{4.375}$	$(\gamma_p < 2)$
$= 2.0 \times 10^{-26} \gamma_p^{0.75}$	$(\gamma_p > 2)$
$\pi^-$ : $\Sigma_{\pi^-}(\gamma_p) = 1.7 \times 10^{-27} (\gamma_p - 1)^{4.375}$	$(\gamma_p < 2)$
$= 1.3 \times 10^{-28} \gamma_p^{3.75}$	$(2 < \gamma_p < 4)$
$= 8.3 \times 10^{-27} \gamma_p^{0.75}$	$(\gamma_p > 4)$

An isotropic proton flux,  $I_p(\gamma_p)$ , ( $\text{cm}^{-2} \text{ s}^{-1} \text{ sr}^{-1} \text{ erg}^{-1}$ ), results in a pion production rate per target proton ( $\text{s}^{-1}$  per proton),

$$q_\pi(\gamma_\pi) = 4\pi \int_{\gamma_{pT}}^{\infty} \Sigma_\pi(\gamma_p) \delta[\gamma_\pi - g(\gamma_p)] I_p(\gamma_p) d\gamma_p. \quad (3)$$

The production rate of secondary quanta, photons and electrons, is determined from  $q_\pi(\gamma_\pi)$  by considering the individual reactions. Neutral pion decay results in two photons, each with energy

$$E_\nu = \frac{1}{2} m_\pi c^2 \left[ \gamma_\pi + (\gamma_\pi^2 - 1)^{1/2} \cos \theta \right], \quad (4)$$

where  $\theta$  is the angle between the momenta of the two photons. The minimum pion energy that can produce a given  $E_\nu$  is

$$\gamma_{\pi, \min}(E_\nu) = \frac{E_\nu}{m_\pi c^2} + \frac{m_\pi c^2}{4E_\nu}. \quad (5)$$

Charged pion decay is more complicated. In the first decay, the neutrino usually takes up the mass energy difference, leaving  $\gamma_\mu = \gamma_\pi$  (Jones 1963). The muon decay results in an electron energy  $\gamma_*$  in the muon rest frame. In the laboratory frame the electron energy is

$$\gamma_e = \gamma_\pi \gamma_* + (\gamma_\pi^2 - 1)^{1/2} (\gamma_*^2 - 1)^{1/2} \cos \theta. \quad (6)$$

The range of  $\gamma_\pi$  which can produce a  $\gamma_e$  is  $\gamma_{\pi, \min} < \gamma_\pi < \gamma_{\pi, \max}$  where

$$\gamma_{\pi, \max}(\gamma_e) = \gamma_* \gamma_e + (\gamma_e^2 - 1)^{1/2} (\gamma_*^2 - 1)^{1/2}. \quad (7a)$$

$$\gamma_{\pi, \min}(\gamma_e) = \gamma_* \gamma_e - (\gamma_e^2 - 1)^{1/2} (\gamma_*^2 - 1)^{1/2}. \quad (7b)$$

The production of secondary products of species  $\alpha$  (photons, positons, negatons) is then ( $\text{s}^{-1}$  per proton)

$$q_\alpha(E_\alpha) = \int_{\gamma_{\pi, \min}(E_\alpha)}^{\gamma_{\pi, \max}(E_\alpha)} q_\pi(\gamma_\pi) f(\gamma_\pi, E) d\gamma_\pi \quad (8)$$

if  $f(\gamma_\pi, E_\nu)$  is the appropriate distribution. For photons, Fazio (1967) gives

$$f(\gamma_\pi, E_\nu) = \left[ m_\pi c^2 (\gamma_\pi^2 - 1)^{1/2} \right]^{-1} \quad (9)$$

for all dynamically allowed  $E_\nu$ . The lower limit of the integral,  $\gamma_{\pi, \min}$ , is given by (5); the upper limit is infinity.

For muon decay, the distribution of electron energies is known in the rest frame:

$$F(\gamma_*) = 2 \left( \frac{2m_e}{m_\pi} \right)^3 \gamma_* (\gamma_*^2 - 1)^{1/2} \left( 3 - \frac{4m_e}{m_\pi} \gamma_* \right) \quad (10)$$

(Jones 1963). Following Ramaty and Lingenfelter, we shall approximate  $F(\gamma_*)$  with a delta function about  $\bar{\gamma}_* = \int F(\gamma_*)\gamma_* d\gamma_* \approx 73.5$ . This leads to the appropriate distribution,

$$f(\gamma_\pi, E_e) = \left[ 2m_e c^2 (\bar{\gamma}_*^2 - 1)^{1/2} (\gamma_\pi^2 - 1)^{1/2} \right]^{-1}, \quad (11)$$

again for all allowed values of  $E_e$ . The limits of integration in (8) become

$$\gamma_{\pi, \max}(\gamma_e) = \gamma_e \bar{\gamma}_* + (\gamma_e^2 - 1)^{1/2} (\bar{\gamma}_*^2 - 1)^{1/2}, \quad (12a)$$

$$\gamma_{\pi, \min}(\gamma_e) = \gamma_e \bar{\gamma}_* - (\gamma_e^2 - 1)^{1/2} (\bar{\gamma}_*^2 - 1)^{1/2}. \quad (12b)$$

Combining (3) and (8), the production rate of secondaries is

$$q_\alpha(E_\alpha) = 4\pi \int_{\gamma_{\pi, \min}(E_\alpha)}^{\gamma_{\pi, \max}(E_\alpha)} f(\gamma_\pi, E_\alpha) \int_{\gamma_{pT}}^{\infty} \Sigma_\pi(\gamma_p) \delta[\gamma_\pi - g(\gamma_p)] I(\gamma_p) d\gamma_p d\gamma_\pi \quad (13)$$

For the photon case, this becomes

$$q_\alpha(E_\alpha) = \frac{4\pi}{m_\pi c^2} \int_{\gamma_{p, \min}(E_\alpha)}^{\infty} \frac{\Sigma_\pi^0(\gamma_p) I_p(\gamma_p) d\gamma_p}{\left[ (\gamma_p - 1)^{3/2} + 2(\gamma_p - 1)^{3/4} \right]^{1/2}}, \quad (14)$$

with

$$\gamma_{p, \min}(E_\alpha) = 1 + \left[ \frac{E_\nu}{m_\pi c^2} + \frac{m_\pi c^2}{4E_\nu} - 1 \right]^{4/3}. \quad (15)$$

The electron production rate is

$$q_{e^\pm}(\gamma_e) = \frac{2\pi}{m_e c^2} \int_{\gamma_{p, \min}(\gamma_e)}^{\gamma_{p, \max}(\gamma_e)} \frac{\Sigma_\pi + (\gamma_p) I_p(\gamma_p) d\gamma_p}{\left[ (\bar{\gamma}_*^2 - 1) \left( 2(\gamma_p - 1)^{3/4} + (\gamma_p - 1)^{3/2} \right) \right]^{1/2}} \quad (16)$$

with

$$\gamma_{p, \max}(\gamma_e) = 1 + \left[ \bar{\gamma}_* \gamma_e + (\bar{\gamma}_*^2 - 1)^{1/2} (\gamma_e^2 - 1)^{1/2} - 1 \right]^{4/3}, \quad (17a)$$

$$\gamma_{p, \min}(\gamma_e) = 1 + \left[ \bar{\gamma}_* \gamma_e - (\bar{\gamma}_*^2 - 1)^{1/2} (\gamma_e^2 - 1)^{1/2} - 1 \right]^{4/3}. \quad (17b)$$

We represent the proton flux by the relativistically correct Maxwellian (Sygne 1957),

$$I_p(\gamma_p) = \left( \frac{2}{\pi} \right)^{1/2} n_p c \left( \frac{m_p c^2}{kT} \right)^{3/2} (\gamma_p^2 - 1) \exp \left[ -(\gamma_p^2 - 1) m_p c^2 / kT \right], \quad (18)$$

in which we have assumed  $T \ll m_p c^2 / k \approx 1.1 \times 10^{13}$  K in order to approximate the modified Bessel function,  $K_2(m_p c^2 / kT)$ . We choose the Maxwellian to represent an ion distribution peaked at a characteristic energy,  $kT_i$ , without meaning to imply that the ion gas has had time to be thermodynamically relaxed. This choice of distribution is the most critical in a plasma with mean energy per proton  $< 290$  MeV ( $T_i = 3.3 \times 10^{12}$  K), for the  $pp$  reactions then involve the high-energy tail of the distribution, and this part of the distribution is the least likely to have relaxed into the Maxwellian.

For the  $pp$  cross section amplitudes we use the forms given in Table 1. These are approximations to curves presented by Stecker (1973) and by Ramaty and Lingenfelter (1966), which make the integrals in (14) and (16) analytic. Calculation of  $q_\nu(E_\nu, T_i)$  and  $q_{e^\pm}(\gamma_e, T_i)$  is then straightforward.

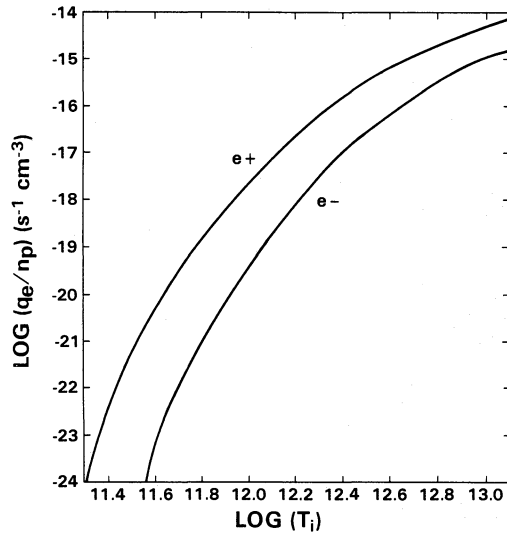


FIG. 1.—The integrated production rate of positrons (*upper curve*) and negatrons (*lower curve*) due to charged pion production in a proton gas at temperature  $T_i$ .

#### b) Decay Product Spectra for a Given $T_i$

The photon number spectrum (photons per second per target particle) from  $\pi^0$  decay is centered at  $E_\nu = m_\pi c^2/2 \approx 70$  MeV. The spectrum we calculate is flat for a range of width  $\sim 150$  MeV (at  $T_i = 3 \times 10^{11}$  K) to 250 MeV (at  $T_i = 3 \times 10^{12}$  K) around the central value, and falls off exponentially on either side of this range. The flat top is due to the artificial form (1); a better calculation will show a rounded top with maximum  $\sim 70$  MeV (cf. Marscher, Vestrand, and Scott 1980). The magnitude of  $q_\nu(E_\nu, T_i)$  is a strong function of  $T_i$ , as one would expect from the cross section given in Table 1 (cf. Dahlbacka, Chapline, and Weaver 1974 for a different formulation).

The electron spectrum resulting from charged pion decay has the same form, namely, a plateau centered on  $\gamma_e = \bar{\gamma}_* = 73.5$  with an exponential decrease in  $q_{e^\pm}(\gamma_e, T_i)$  at higher and lower  $\gamma_e$ . Figure 1 shows the integrated electron production rate,

$$q_{e^\pm}(T_i) = \int q_{e^\pm}(\gamma_e, T_i) d\gamma_e. \quad (19)$$

Again the strong dependence on  $T_i$  is evident. The dominance of positron production over negatron production at lower proton energies is reflected in the smaller  $q_{e^-}(T_i)$  values, compared to  $q_{e^+}(T_i)$ .

Penrose processes in a disk about a rotating black hole will contribute a small number of more energetic particles, up to 1 GeV. As these effects involve the interaction of disk photons with the ergosphere of the black hole, we reserve discussion of this for the next section.

#### c) Total X- and $\gamma$ -Ray Spectrum

We consider four sources of hard photons relevant to accretion disk material at ion temperature  $T_i$  and electron temperature  $T_e$ . Figure 2 shows the emission spectrum integrated over radius in an optically thin model disk, broken up into the four components.

The spectral emissivity (ergs  $s^{-1}$  erg $^{-1}$ ) of this process can be found as a solution of the Kompaneets equation (cf. Rybicki and Lightman 1979, or SLE),

$$\epsilon_e(E_\nu) = \epsilon_0 \nu^{a(y, T_e)} \exp(-h\nu/kT_e), \quad (20a)$$

where, if  $y = (kT/mc^2) \max(\tau_{es}, \tau_{es}^2)$  and  $\tau_{es}$  is the electron scattering optical depth, the spectral index is

$$a(y, T_e) = \frac{3}{2} \left\{ 1 - \left[ 1 + \frac{16}{9y(1+f)} \right]^{1/2} \right\} \quad (20b)$$

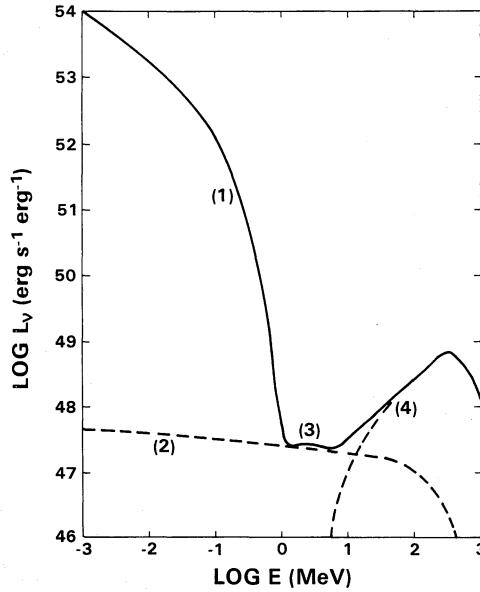


FIG. 2.—The photon spectrum from a disk model with  $\dot{M} = 1 M_{\odot} \text{ yr}^{-1}$ ,  $M = 10^8 M_{\odot}$ ,  $a = 0.1$ ,  $y = 1$ . This is the spectrum emitted by an optically thin disk; that seen at infinity is affected by relativistic effects, and is given in Fig. 5. Optical depth effects modify the spectrum, as shown in Fig. 3. Component (1) is unsaturated Compton electron cooling; (2) is bremsstrahlung from relativistic electrons created in pion decay; (3) is the 4.4 MeV line of carbon; (4) is from neutral pion decay. The disk spectrum is very close to that of an ion gas at a single temperature equal to the maximum disk  $T_i$ .

with

$$f = 2.5\theta + 1.875\theta^2(1 - \theta)$$

if  $\theta = kT_e/m_e c^2$ . This spectral index is quite sensitive to  $y$  if  $y \geq 1$ . The height of the spectrum is determined by requiring the total electron cooling (see § III) to equal the spectrum (20), integrated over frequency, with an arbitrary low-energy cutoff  $\nu_0 = 10^{15}$  Hz. The constant  $\epsilon_0$  is sensitive to  $\nu_0$  only if  $y < 1$  ( $|a| > 1$ ), in which case  $\epsilon_0 \propto \nu_0(|a| - 1)$ .

Radiation from the relativistic electrons provides the second component of the spectrum. These electrons are unlikely to be trapped in the disk. The lifetime for a 35 MeV electron to annihilation, bremsstrahlung losses, or Coulomb losses in the disk is longer than the escape time,  $h/c$  in a disk of half-thickness  $h$ . Thus, a simple estimate of the density of relativistic electrons is

$$n_{e^{\pm}}(\gamma_e, T_i) = q_{e^{\pm}}(\gamma_e, T_i) n_p h / c. \quad (21)$$

Three factors may change this simple density estimate. If plasma microturbulence reduces the particle streaming speed much below  $c$ ,  $n_{e^{\pm}}$  will be larger than given by (21). If the relativistic particles suffer severe inverse Compton losses on the cold photons, their annihilation lifetime shortens and (21) will be a poor estimate of their density. Finally, if  $\gamma\gamma$  pair production is important (cf. Cavallo and Rees 1978; Liang 1979), the pair density may exceed the estimate (21). Considering all three effects, we expect that (21) is a conservative estimate of the energetic particle density.

Bremsstrahlung or Comptonization will be the strongest radiation mechanism from these electrons. We calculate the bremsstrahlung directly from (21), using the ion density in the disk, noting that for electrons of energy  $\gamma_e m_e c^2$ , the spectrum has the usual cutoff at  $E_\nu \approx \gamma_e m_e c^2$ . Integrating over electron energies gives the total emissivity,  $\epsilon_{\text{ff}}(E_\nu)$ , component (2) in Figure 2. The height of  $\epsilon_{\text{ff}}(E_\nu)$  depends strongly on  $T_i$ , reflecting the  $q_{e^{\pm}}(T_i)$  behavior of Figure 1. We do not attempt to model the Compton losses of the relativistic electrons in detail but note that these losses can enhance the hard X-ray spectrum (cf. Caroff, Eilek, and Noerdlinger 1983).

A third  $\gamma$ -ray emissivity is due to excited nuclear lines. We include emission from one line, the 4.4 MeV line of carbon (component 3 in Fig. 2). Higdon and Lingenfelter (1977) give the total emissivity in this line as a function of temperature. We do not compute a line profile, but note that the  $\text{FWHM} \approx 0.9 T_{i,12}^{1/2}$  MeV, which is slightly less than our frequency grid in the numerical work. This line is visible at intermediate  $T_i$ ; below  $T_i \sim 10^{12}$  K the line is very weak,



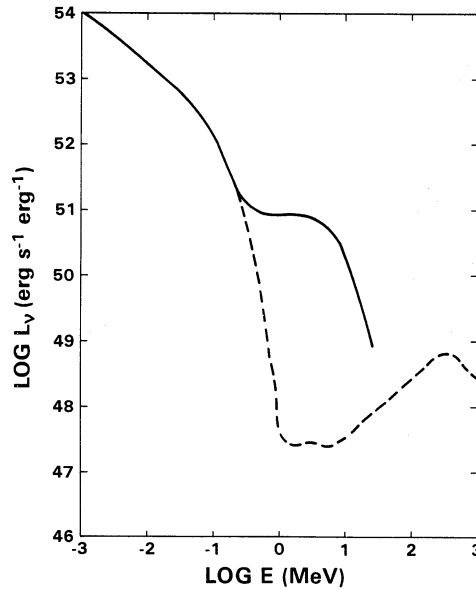


FIG. 3.—Expected spectrum for the model in Fig. 2 due to opacity to pair production above  $\sim 6$  MeV

and above  $T_i \sim 5 \times 10^{12}$  K the bremsstrahlung from the relativistic electrons swamps the line. The 0.5 MeV annihilation line has a FWHM  $\approx 1.1T_4^{1/2}$  keV (Crannell, Joyce, and Ramaty 1976). Any contribution to this line from the disk itself will be swamped by the thermal component (1). If the positrons escape the disk and annihilate in an ambient gas, we estimate from our higher- $L_\gamma$  models that the line will be observable above the continuum if the ambient temperature  $\leq 10^7$  K.

Finally, the dominant  $\gamma$ -ray emission is the peak at 100–200 MeV from  $\pi^0$  decay (component 4 in Fig. 2). The emissivity in this mode is given by  $\epsilon_{\pi^0}(E_\nu, T_i) = n_p q_\nu(E_\nu, T_i)$  from (14). The strength of this peak depends on  $T_i$ : for  $T_i \geq 1 \times 10^{12}$  K, the flux in the  $\pi^0$  peak exceeds  $10^{-3}$  of the total flux (almost all in component 1); for  $T_i > 3 \times 10^{12}$  K, the  $\pi^0$  flux exceeds 1% of the total; for  $T_i$  reaching  $10^{13}$  K—the highest  $T_i$  for which these models are valid— $\pi^0$  flux reaches 10% or more of the total flux.

We note, finally, that many of the models turn out to be optically thick to  $\gamma\gamma$  pair production for photon energies above a few MeV. This will degrade the 100 MeV  $\gamma$ -ray peak to a few MeV, and the disk spectrum will not look like Figure 2 but rather will have a knee at a few MeV. We do not attempt to model this secondary spectrum in detail, as such an extensive calculation (Caroff, Eilek, and Noerdlinger 1983) is outside the scope of this paper. In Figure 3, however, we indicate the approximate shape of the optically thick spectrum from the model of Figure 2. We assume that all the luminosity above the smallest optically thick photon energy,  $E_{\gamma\gamma}$ , is degraded to or below  $E_{\gamma\gamma}$ , with a spectral shape below  $E_{\gamma\gamma}$  that is constant or decreasing toward lower energy.

### III. DISK MODELS AND THEIR SPECTRA

#### a) Calculating the Disk Structure

Having determined the photon and electron production rates as a function of ion temperature, we next compute accretion models. We use the optically thin, unsaturated Compton disk model of SLE (which is critically discussed by Eardley *et al.* 1978, and also by LT), as extended to a Kerr metric in Paper I. In common with most disk accretion models (cf. Novikov and Thorne 1973) this model assumes a Keplerian azimuthal velocity,  $v_\phi$ , with a slow inward drift,  $v_r$ , determined by viscous dissipation. The viscosity is parameterized such that the viscous stress is given by  $\alpha p$ , if  $p$  is the gas pressure and  $0 < \alpha \leq 1$ . This assumption, that  $v_r \ll v_\phi$ , breaks down in the inner regions of a Kerr disk (Paper I and Kafatos and Leiter 1979). Liang and Thompson (1980) have looked at transonic disk accretion in isothermal flows and in unsaturated Compton flows with  $T_i/T_e$  held constant. We are presently extending this work to accretion in a Kerr metric. For the present work, however, we shall retain the Keplerian  $\alpha$ -disk.

The thermal structure of the gas is the important property of the model. Disk accretion apparently can occur in more than one mode. One such mode is a cool, optically thick disk, radiating at its blackbody temperature,  $T_{bb} \approx 10^6$

TABLE 2  
APPROXIMATE EQUATIONS DESCRIBING DISK STRUCTURE

$$\begin{aligned}
 & \tau_{\text{es}} < 1: \\
 & \tau_{\text{es}} = 3.3 \alpha^{1/6} y^{1/2} \left( \frac{\dot{M}_\star}{M_8} \right)^{1/6} \left( \frac{f_3^2}{f_1 f_2} \right)^{1/6} \frac{1}{r_\star^{1/4}} \\
 & T_i = \frac{1.5 \times 10^{13} \text{ K}}{\alpha^{7/6} y^{1/2}} \left( \frac{\dot{M}_\star}{M_8} \right)^{5/6} \left( \frac{f_2^7 f_1}{f_3^2} \right)^{1/6} \frac{1}{r_\star^{5/4}} \\
 & T_e = 4.2 \times 10^8 \text{ K} \frac{y^{1/2}}{1/6} \left( \frac{M_8}{\dot{M}_\star} \right)^{1/6} \left( \frac{f_1 f_2}{f_3^2} \right)^{1/6} r_\star^{1/4} \\
 & n = 2.9 \times 10^{11} \text{ cm}^{-3} \frac{\alpha^{3/4} y^{3/4}}{M_8} \left( \frac{M_8}{\dot{M}_\star} \right)^{1/4} \left( \frac{f_1 f_3^2}{f_2^3} \right)^{1/4} \frac{1}{r_\star^{9/4}} \\
 & \frac{h}{r} = \frac{1.2}{\alpha^{7/12} y^{1/4}} \left( \frac{\dot{M}_\star}{M_8} \right)^{5/12} \left( \frac{f_2^7}{f_1^5 f_3^2} \right)^{1/12} \frac{1}{r_\star^{1/8}} \\
 & \tau_{\text{es}} > 1: \\
 & \tau_{\text{es}} = 2.2 \alpha^{1/9} y^{1/3} \left( \frac{\dot{M}_\star}{M_8} \right)^{1/9} \left( \frac{f_3^2}{f_1 f_2} \right)^{1/9} \frac{1}{r_\star^{1/6}} \\
 & T_i = \frac{2.3 \times 10^{13} \text{ K}}{\alpha^{10/9} y^{1/3}} \left( \frac{\dot{M}_\star}{M_8} \right)^{8/9} \left( \frac{f_1 f_2^{10}}{f_3^2} \right)^{1/9} \frac{1}{r_\star^{4/3}} \\
 & T_e = 2.9 \times 10^8 \text{ K} \frac{y^{1/3}}{\alpha^{2/9}} \left( \frac{M_8}{\dot{M}_\star} \right)^{2/9} \left( \frac{f_1^2 f_2^2}{f_3^4} \right)^{1/9} r_\star^{1/3} \\
 & n = 1.5 \times 10^{11} \text{ cm}^{-3} \frac{\alpha^{2/3} y^{1/2}}{M_8} \left( \frac{M_8}{\dot{M}_\star} \right)^{1/3} \left( \frac{f_1 f_3}{f_2^2} \right)^{1/3} \frac{1}{r_\star} \\
 & \frac{h}{r} = \frac{1.5}{\alpha^{5/9} y^{1/6}} \left( \frac{\dot{M}_\star}{M_8} \right)^{4/9} \left( \frac{f_2^5}{f_1^4 f_3} \right)^{1/9} \frac{1}{r_\star^{1/6}}
 \end{aligned}$$

$K(\dot{M}/M_\odot \text{ yr}^{-1})(M/10^8 M_\odot)^{-2}$ . Another is a hot, optically thin model where the temperature is determined by the specific cooling mechanisms of the electrons and ions. Assuming that unsaturated Comptonization from an external source of soft photons cools the electrons, and that only Coulomb collisions with the electrons allows the ions to cool, then viscous ion heating leads to the two-temperature disk of SLE. Large values of  $\dot{M}/M$  then result in heating strong enough to cause  $T_i \gg T_e$ .

It is of course possible that a stronger microscopic coupling can thermalize the two distributions (although no specific mechanism has been proposed). Assuming  $T_i = T_e$  leads to models such as the coronal model of Liang and Price (1977), and LT. This assumption leads to an equilibrium temperature intermediate between  $T_i$  and  $T_e$  in the two-temperature model.

In this paper, however, we assume only Coulomb coupling between the ions and electrons. In order to calculate disk models we use six structure equations involving  $T_i$ ,  $T_e$ ,  $p$ , the density  $n$ , the disk half-thickness  $h$ , and the optical depth  $\tau_{\text{es}}$ . The parameters  $\alpha$  (viscosity) and  $y$  (Comptonization) are varied slightly in the solutions. As these equations are not new, we defer listing them and describing the solution in detail to the Appendix. We do include cooling from pion production in the ion thermal equation. We note that pion production from  $pp$  collisions is the next most important proton cooling mechanism after Coulomb collisions with electrons. Other reactions available to medium-energy protons—spallation,  $pp$  bremsstrahlung, or direct pair production ( $pp$ ,  $pe$ , or  $p\gamma$ ) have lower cross sections than pion production, and also may have low rates due to the lower abundances of heavy elements or photons with  $h\nu > 2m_e c^2$ .

In general the solution involves numerical solution of an algebraic equation for  $\tau_{\text{es}}$ . However, when  $T_i > T_e$  and when the pion cooling is negligible, approximate analytic solutions can be found in the two regimes,  $\tau_{\text{es}} \gg 1$ . These are presented for reference in Table 2; the numerical solutions deviate from these as  $T_i$  approaches  $T_e$  or as the pion cooling becomes important. Figure 4 shows the radial behavior of temperature and density for one particular model in Schwarzschild and canonical Kerr ( $a_\star = 0.998$ ) metrics (Thorne 1974).

The dependence of  $T_i$  on the disk parameters is important. The disk in the canonical Kerr metric extends inwards to  $r_{\text{ms}} = 1.2 r_g$  ( $r_g = GM/c^2$ ), with  $T_i$  reaching a maximum at  $r \approx 2r_g$ , whereas the Schwarzschild disk extends only to  $6r_g$  and has maximum  $T_i$  at  $r \approx 12r_g$ . We see from Table 2 that  $T_i$  depends on the ratio  $\dot{M}/M$ , rather than on  $\dot{M}$  and  $M$

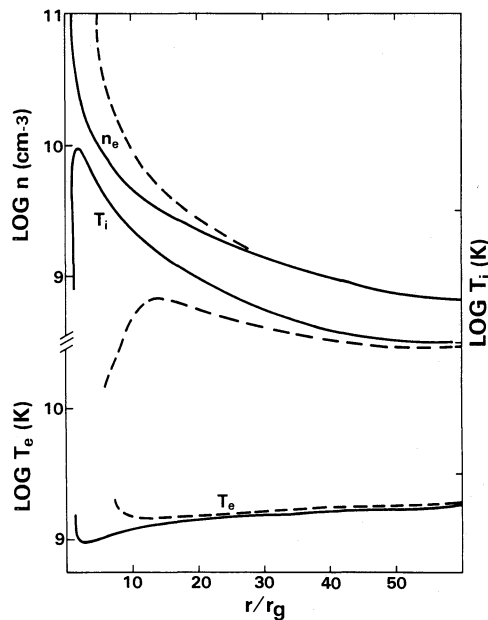


FIG. 4.—Temperature and density behavior in an accretion disk with  $\dot{M}=1 M_{\odot} \text{ yr}^{-1}$ ,  $M=10^8 M_{\odot}$ ,  $\alpha=0.1$ . The solid line is the canonical Kerr model; the dotted line is the Schwarzschild case.  $r_* = r/1.5 \times 10^{13} \text{ cm}$ .

independently, and inversely on fractional powers of the parameters  $y$  and  $\alpha$ . Table 3 summarizes the Kerr models we calculated using  $a_* = 0.998$ . In this table we list the “independent variables,”  $\dot{M}/M$ ,  $\alpha$ ,  $y$ , and the calculated values for  $T_{i, \text{max}}$ , the  $\gamma$ -ray luminosity  $L_{\gamma}$ , for the optically thin case, the X-ray luminosity  $L_e$  (from Compton cooling), the relativistic electron production rate  $\dot{N}_e$ , and the photon energy above which the opacity to  $\gamma$ - $\gamma$  pair production exceeds unity,  $E_{\gamma\gamma}$  (see § IIIb). We note that these ranges of  $\dot{M}/M$  are consistent with the condition for the existence of an inner, optically thin, “hot” disk,  $\dot{M}/M \geq 10^{-10} \alpha^{-17/32} (M/10^8 M_{\odot})^{-1/32} \text{ yr}^{-1}$  (Eardley and Lightman 1975; Kafatos 1980). We find empirically that  $T_{i, \text{max}} > 10^{12}$  for  $\dot{M}/M > 3 \times 10^{-9} \alpha y^{1/2} \text{ yr}^{-1}$  in the Kerr metric, and for  $\dot{M}/M > 8 \times 10^{-8} \alpha y^{1/2} \text{ yr}^{-1}$  in the Schwarzschild metric. In disks which are optically thick—those with  $E_{\gamma\gamma}$  as low as a few MeV—the emergent  $\gamma$ -ray luminosity will be the sum of  $L_{\gamma}(\text{thin})$  and the energy flux in electrons,  $L_{e\pm} \approx L_{\gamma}(\text{thin})$ . The models with  $\dot{M}/M = 3 \times 10^{-8} \text{ yr}^{-1}$  and  $\alpha = 0.1$  should not be taken very seriously. They show  $T_i \gg m_p c^2$  (in violation of our assumptions in § IIa) and  $L_e \gg L_{\text{Edd}}$ ; we include them to indicate the limit of self-consistency of these calculations. Pion production is significant in these hot models. The fact that  $T_i$  depends only on the ratio  $\dot{M}/M$  means that galactic X-ray sources—those due to accretion onto stellar-sized black holes—will also be seen as  $\gamma$ -ray sources if  $\dot{M}/M$  is high enough.

Disks associated with slowly rotating or stationary black holes tend to be less interesting as a source of  $\gamma$ -rays or energetic particles. This is because the innermost stable orbit, which provides the inner edge of the accretion disk in traditional models, is farther from the hole. This reduces the maximum  $T_i$ , and hence the importance of the high-energy processes, compared to a rapidly rotating hole with the same accretion rate.

It is hard to say whether accreting gas will choose an optically thick or optically thin mode. We feel that the outer boundary conditions of the disk—i.e., the “pre-disk” state of the gas—probably select the hot or cold mode. (For instance, Pringle, Rees, and Pacholczyk 1973 suggest that a tenuous gas may be adiabatically heated in quasi-spherical infall before it can radiate and before it forms into a disk.) On the other hand, it is often assumed that the gas, at least in the inner regions, will form into a cold, optically thick disk, and then undergo a phase transition to the hot mode. SLE suggest that the secular instability (Lightman and Eardley 1974) will set off a thermal instability (e.g., Pringle 1976) and cause the transition. Stoeger (1980) disagrees with this but suggests that a density gradient due to a radial velocity gradient can trigger the transition. The thermal stability of the hot disk phase is problematic. Piran (1978) has shown that both bremsstrahlung and Compton cooled disks are thermally unstable when the heating is given by the  $\alpha$ -viscosity. A thermal instability in a cold disk will not, of course, induce a transition to the hot phase if that phase is itself unstable. LT suggest that a corona with the cooling modulated by thermal conduction will be thermally stable. However, the change in thermal conductivity at high temperatures will induce thermal instability in this model also. (A

TABLE 3  
DISK MODELS WITH KERR METRIC

$\dot{M}/M$ (yr <sup>-1</sup> )	$y$		max $T_i$ (K)	$L_\gamma/L_e$	$L_e/L_{\text{Edd}}$	$\dot{N}_e/\dot{M}$	$E_{\gamma\gamma}$ (MeV)	
$3 \times 10^{-10}$ .....	0.1	0.3	2.4(12)	3.9(-3)	4.4(-2)	2.6(-2)	200	
		3.0	8.6(11)	4.5(-5)	4.3(-2)	1.5(-3)	30	
	1.0	0.3	1.7(11)	3.2(-9)	4.1(-2)	5.1(-11)	300	
		3.0	6.5(10)	6.9(-10)	4.1(-2)	...	60	
$10^{-9}$ .....	0.1	0.3	6.6(12)	3.0(-2)	0.15	0.16	300	
		1.0	3.4(12)	2.0(-2)	0.17	0.13	15	
		3.0	2.3(12)	1.0(-2)	0.18	8.0(-2)	3	
		1.0	0.3	4.6(11)	8.7(-8)	0.14	4.2(-6)	400
	1.0	1.0	2.8(11)	2.3(-8)	0.14	1.2(-7)	30	
		3.0	1.9(11)	1.3(-8)	0.14	1.6(-9)	10	
		0.1	0.3	1.7(13)	8.1(-2)	9.6(-2)	0.31	300
		1.0	1.0	9.5(12)	8.3(-2)	0.46	0.43	10
$3 \times 10^{-9}$ .....	0.1	3.0	6.5(12)	7.7(-2)	0.51	0.47	3	
		1.0	0.3	1.1(12)	2.6(-5)	0.41	3.9(-4)	400
		1.0	1.0	7.4(11)	2.3(-6)	0.41	9.9(-5)	10
	1.0	3.0	5.1(11)	4.3(-7)	0.41	2.2(-5)	5	
		0.1	0.3	4.6(13)	0.24	1.4	0.53	400
		1.0	1.0	2.8(13)	0.25	1.4	0.75	6
		3.0	1.9(13)	0.25	1.5	0.96	4	
		0.3	3.2(12)	2.2(-3)	1.4	1.3(-2)	500	
$10^{-8}$ .....	1.0	1.0	2.2(12)	1.1(-3)	1.4	7.0(-3)	6	
		3.0	1.5(12)	3.1(-4)	1.4	3.0(-3)	5	
		0.1	0.3	1.1(14)	0.48	4.2	0.75	200
	0.1	1.0	7.4(13)	0.65	4.2	1.1	4	
		3.0	5.2(13)	0.70	4.3	1.5	2	
		1.0	0.3	8.6(12)	9.4(-3)	4.2	4.5(-2)	300
		1.0	1.0	5.8(12)	9.3(-3)	3.9	4.8(-2)	8
		3.0	3.9(12)	7.4(-3)	3.9	4.3(-2)	2	

classical collisional gas has conductive heat flux  $\propto T^{5/2} \nabla T$ , but the heat flux tends to saturate when the gas becomes collisionless and/or relativistic; cf. Eilek and Caroff 1979.) On the other hand, Piran points out that a change in the heating law from the arbitrary constant- $\alpha$  form can be stabilizing. In particular, a viscosity parameter  $\alpha'$  proportional to  $(nh)^{-m}$ , with  $m > 1$ , is stabilizing. [This form comes from Piran's analysis in terms of  $d \ln \alpha / d \ln (nh)$ , and not, we emphasize, from any physical argument about dissipation.]

We feel that both the "choice" of the accreting gas for a hot or cold phase, and the thermal stability of a true hot phase, are unanswered questions at the present. The hot, two-temperature model still seems to be physically possible in the light of these arguments.

#### b) High-Energy Spectra from These Models

The  $\gamma$ -ray spectrum from a disk is dominated by that region of the disk where  $T_i$  is highest. We can see directly from Table 3 that the disk parameters ( $\dot{M}/M$ ,  $\alpha$ ,  $y$ ) determine  $T_{i, \text{max}}$  and hence  $L_\gamma$ , the total luminosity due to pion processes, and  $\dot{N}_e$ , the particle production rate from pion processes.

Figure 2 shows the photon spectrum (as seen at the disk) for one of the models with high  $\gamma$ -ray flux:  $M = 10^8 M_\odot$ ,  $\dot{M} = 1 M_\odot \text{ yr}^{-1}$ ,  $\alpha = 0.1$ . The spectrum from this disk, observed at infinity (Cunningham 1975) is shown in Figure 5 at three observing angles. The factor of 2 or 3 shift in the  $\gamma$ -ray peak is worth noting. The  $\pi^0 \rightarrow 2\gamma$  peak and also the  $e^\pm$  bremsstrahlung spectrum shown in Figures 2 and 5 depend strongly on  $T_{i, \text{max}}$ . In Figure 6 we show  $L_e/L_{\text{Edd}}$  and  $L_\gamma/L_e$  as a function of  $\dot{M}/M$ , with  $\alpha = 0.1$  and 1.0, for both Schwarzschild and canonical Kerr models.  $L_e$  is the total electron cooling of the disk, given by energy conservation by the second term in equation (A4), and  $L_{\text{Edd}}$  is the classical Eddington luminosity,  $L_{\text{Edd}} = 1.3 \times 10^{46} M_8 \text{ ergs s}^{-1}$ . For the highest  $\dot{M}/M$  values,  $L_e > L_{\text{Edd}}$ , and the model as calculated may be inconsistent (see, however, Liang 1979). In all models calculated,  $L_e/\dot{M}c^2 < 0.42$ , the extreme Kerr limit (Bardeen, Press, and Teukolsky 1972). However, for  $\dot{M}/M$  high enough that  $T_{i, \text{max}} > 10^{12} \text{ K}$  but still sub-Eddington, the pion-induced  $\gamma$ -ray luminosity is appreciable. The most interesting cases result in  $L_\gamma \approx 0.1 L_e$ , that is, in 10% of the total luminosity being in the  $\gamma$ -ray band. As one would expect from the dependence of  $T_{i, \text{max}}$  on the model parameters, rotating black holes and lower disk viscosities favor higher  $\gamma$ -ray production. This result can be very significant for models of active nuclei especially, where  $\dot{M}/M \sim 10^{-8} \text{ yr}^{-1}$  is generally considered.

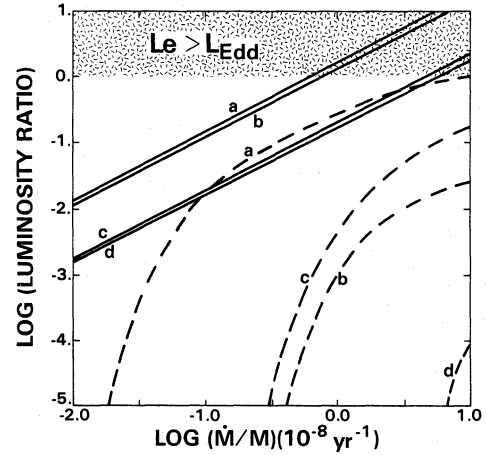
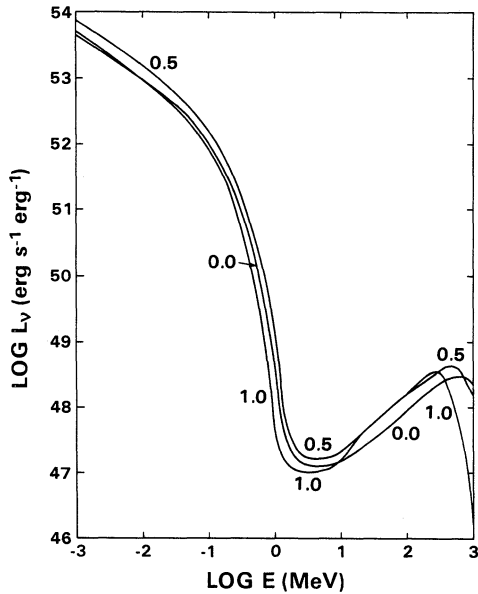


FIG. 5.—The total spectrum from the disk of Fig. 2, as seen at infinity. The labels specify the cosine of the observing angle (where observers have a cosine of unity, and equatorial observers have a cosine of zero).

FIG. 6.—*Solid line*, total electron cooling,  $L_e$ , as a fraction of the Eddington luminosity,  $L_{\text{Edd}} = 1.3 \times 10^{46} M_8 \text{ ergs s}^{-1}$ . *Dotted line*, total pion-induced luminosity of  $L_e$ . The curves are for (a) canonical Kerr,  $\alpha = 0.1$ ; (b) canonical Kerr,  $\alpha = 1.0$ ; (c) Schwarzschild,  $\alpha = 0.1$ ; (d) Schwarzschild,  $\alpha = 1.0$ .

The Comptonization parameter  $y$  can strongly affect the X-ray spectrum, as shown in equation (20). This change is much more significant than the slow dependence of the disk structure parameters on  $y$  (cf. Table 2). In Figure 7 we show the same disk model as in Figure 2, but with  $y$  varying from 0.3 to 3.0. The change in the X-ray spectrum is striking. The conventional choice in the literature has been  $y \approx 1$ , which agrees with observed X-ray spectra of galactic objects. It has been argued that a steady state system will have  $y \approx 1$  because the strong dependence of the electron cooling on  $y$  when  $y \geq 1$  will act as a thermostat (cf. SLE; Holt and McCray 1982). We continue this choice, but note the extreme sensitivity of the X-ray slope, and also of the pair production opacity (discussed immediately below) to small changes in  $y$  when  $y \approx 1$ .

This calculation indicates that most of the  $\gamma$ -ray and X-ray luminosities are emitted in the inner region of the disk,  $r \leq 50 r_g$ , say. This means that the photon density in the more luminous models is high enough that pair production in  $\gamma$ -ray photon-X-ray photon interactions is important. (McBreen 1979 has pointed this out for 3C 273.) We list in Table 3 the frequency,  $E_{\gamma\gamma}$ , at which  $\tau_{\gamma\gamma} \sim 1$  (calculated perpendicular to the disk) for pair production from the X-ray spectrum, assuming the X-ray photons are spread evenly over a region  $\sim 20 r_g$  and are isotropically distributed. Photons with  $E \geq E_{\gamma\gamma}$  cannot escape the region. In Figure 8 we show the frequency dependence of the photon mean free path,  $l(\nu)$ , for several models. We find that  $E_{\gamma\gamma}$  [chosen, for instance, so that  $l(E_{\gamma\gamma}) = 20 r_g$ ] is sensitive most strongly to the Comptonization parameter  $y$ . For  $y > 1$ ,  $E_{\gamma\gamma} \sim 3\text{--}10$  MeV, with little sensitivity to the other model parameters. For  $y < 1$ , however,  $E_{\gamma\gamma} > 100$  MeV, reflecting the steeper X-ray spectrum and the relative absence of photons above the energy threshold for pair production. Models with  $E_{\gamma\gamma}$  as low as a few MeV will not display the optically thin spectrum calculated in this paper, but rather will modify that spectrum through pair production and annihilation processes, as illustrated in Figure 3.

The rate of energetic particle production, calculated from equation (16), is shown in Figure 9 as a function of  $\dot{M}/M$ , again for a range of  $(y, \alpha)$  values. The disk models which produce the highest  $\gamma$ -ray luminosities,  $L_\gamma/L_e \geq 0.11$  (Fig. 6), also have total relativistic particle production rates,  $\dot{N}_e \geq 0.1\dot{M}$  if  $\dot{M}$  is measured in protons per second. We note again that second order effects—viz.,  $\gamma\gamma$  pair production and cascade—will increase the particle production.

Another possible source of energetic particles is  $\gamma$ - $p$  pair production in the ergosphere of a Kerr black hole, which can result in an ejected pair with total energy up to  $m_p c^2$ . This is the Penrose process, suggested for massive black holes by Leiter and Kafatos (1978) and Kafatos and Leiter (1979). This process involves a photon with energy  $h\nu \geq 1$  MeV colliding with a proton in the ergosphere ( $r < 2r_g$  for a canonical Kerr metric). The  $\gamma + p \rightarrow p + e^+ + e^-$  reaction

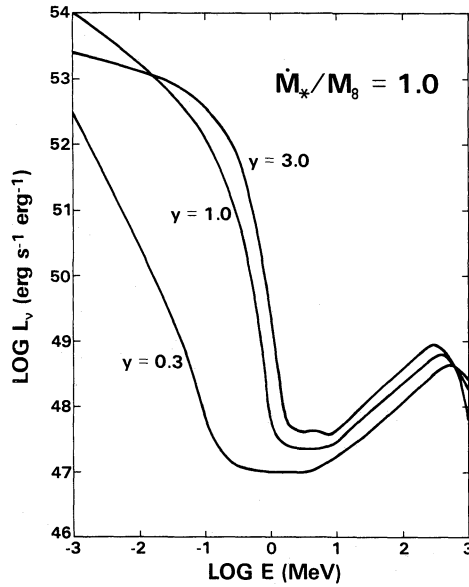


FIG. 7.—The effects of the Comptonization parameter,  $\gamma$ , on the model of Fig. 2. We note the sensitivity of the X-ray slope below  $\sim 300$  keV to small changes in  $\gamma$ .

products may fall into the hole, or they have some chance of escaping with added energy. We are not aware of detailed calculations for this process, but Piran and Shaham (1977) have done Monte Carlo simulations of Compton scattering in the ergosphere. Their results indicate that about 20% of the collisions result in an escaping high-energy photon. The escaping spectrum declines faster than a power law but less fast than an exponential, and has a peak at an energy a few times  $E_0$  if  $E_0$  is the initial photon energy. As in Figure 5, the spectra are harder for angles close to the equatorial plane.

Penrose Compton scattering boosts photons to  $E \sim 1$  MeV, but will be swamped by the other  $\gamma$ -ray production in these models. We investigated Penrose pair production in some detail, however. As it depends on the total  $\gamma$ -ray luminosity of the disk, we did not include this process in the model, but rather estimate its magnitude *ex post facto*. The

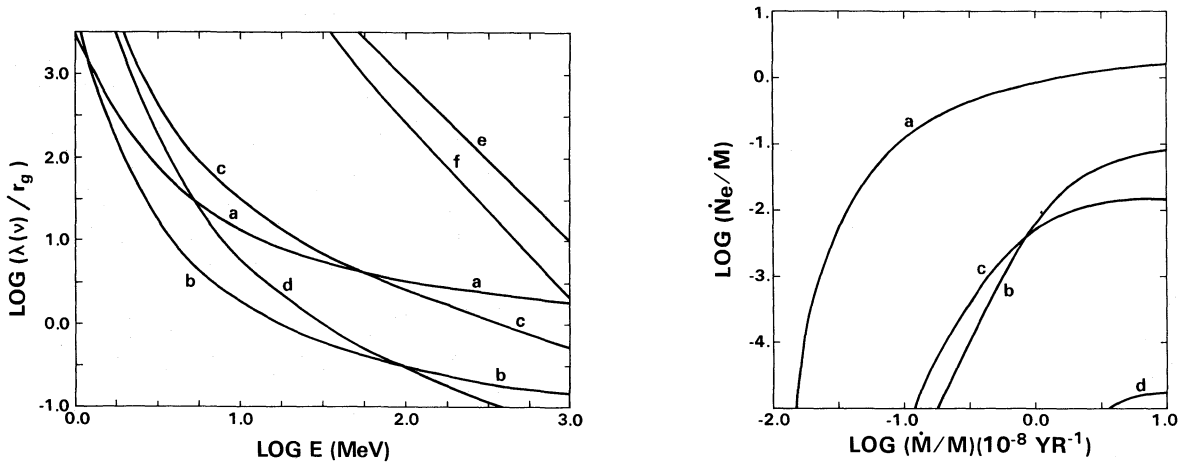


FIG. 8.—The mean free path,  $l(\nu)$  (in units of  $r_g = GM/c^2$ ) for a photon of frequency  $\nu$  to pair production with other disk-created photons. The dotted line marks  $20 r_g$ , to give an estimate for the mean free path needed to escape.

FIG. 9.—The particle creation rate,  $N_e$  (in units of  $s^{-1}$ ), in terms of the mass accretion rate,  $\dot{M}_*$  (in units of  $M_\odot \text{ yr}^{-1}$ ). The labels refer to the models of Fig. 5.

probability of a photon from the disk hitting the ergosphere is given by the fractional solid angle ( $\sim hr_g/r^2$  for  $r \gg r_g$ ), increased by the capture cone for the rotating hole. We estimated the pair-production optical depth for a photon in the ergosphere:

$$\tau_{\text{erg}} = \int_{r_{\text{ms}}}^{2r_g} \sigma_{\gamma p} n(r) e^{\mu_1} dr.$$

(Cf. Kafatos and Leiter 1979 for  $e^{\mu_1}$ , and Paper I for  $\sigma_{\gamma p}$ .) The optical depth was in the range 0.03–1.1 for the models calculated. We assumed that 0.2 of the photons undergoing pair production in the ergosphere result in an escaping pair. We estimated the Penrose pair production rate from  $\tau_{\text{erg}}$ , using the calculated  $L_\gamma$ . We combined  $\tau_{\text{erg}}$  with the fractional solid angle given above, and with the calculated  $L_\gamma$  for various models to estimate the Penrose pair production rate. We found  $\dot{N}_{ppp}/\dot{N}_e \sim 10^{-4}$  to  $10^{-3}$  for all models. The increased probability of capture for photons created near the ergosphere may raise this a bit; we expect the most favorable situation would give  $\dot{N}_{ppp}/\dot{N}_e \sim 10^{-2}$ . This means the luminosity in Penrose pairs (at 1 GeV per pair) may be from a few percent to 10% of  $L_\gamma$  from the disk.

#### IV. DISCUSSION AND CONCLUSIONS

We have found that the two-temperature accretion disk proposed by Shapiro, Lightman, and Eardley (1976) can be a strong source of  $\gamma$ -rays and relativistic particles. The important results of the calculation are as follows.

- i) The  $\gamma$ -ray luminosity can be a significant part of the total disk luminosity. A high  $L_\gamma$  is favored in models with  $\dot{M}/M \geq 3 \times 10^{-9} \alpha y^{1/2} \text{ yr}^{-1}$  in a canonical Kerr metric (high  $\dot{M}/M$  values are required in the Schwarzschild case).
- ii) The inner region will be optically thick to the higher energy  $\gamma$ -rays in models with flat X-ray spectra (those with  $y \geq 1$ ). Cascade interactions between photons and particles will degrade the higher-energy spectrum down to 1–10 MeV in these disks.
- iii) The high-energy spectrum will consist of a power law spectrum out to a few hundred keV (from unsaturated Compton cooling of electrons at  $T_e \geq 10^9$  K) and a  $\gamma$ -ray component which can be as large as 10–20% of the total luminosity. The  $\gamma$ -ray emission is a “knee” at a few MeV in the optically thick models, and a peak at a few hundred MeV in the optically thin models.
- iv) The high- $\dot{M}/M$  models are also strong sources of relativistic positons and negatons at  $\sim 50$  MeV per particle, with the energy flux in these particles comparable to  $L_\gamma$ .
- v) Penrose pair production does occur in the ergosphere, with an energy flux  $\sim 1$ –10% of the energy flux of particles from primary pion reactions.

The particle fluxes predicted are not directly observable, although the particles may act as a source for radio emission (cf. Paper I) and the positrons will produce annihilation radiation (the strength and spectrum of which will depend on local conditions). The hard X-ray and  $\gamma$ -ray flux is observable and may test the validity of the model. How do these models compare with the few observations we have?

##### a) Galactic Sources

Few galactic sources have been detected above 100 keV, except for the transient and bursting sources which are unlikely to be explained by the present model. However, Nolan *et al.* (1981) have measured the high-energy spectrum of Cyg X-1 out to 10 MeV and find a significant excess flux (5–10% of the total power) for 300 keV to 1 MeV, as compared to a single-temperature thermal spectrum at  $kT_e = 32$  keV. Their energy spectrum below 200 keV can be fitted with a power law proportional to  $E^{-0.5}$ . Both this relatively flat X-ray slope and the excess emission above 300 keV, with a cutoff at a few MeV, agree well with our optically thick models.

The other striking galactic source is, of course, the galactic center. In addition to a compact nonthermal radio source (Lo 1982), the region shows continuous hard X-ray emission out to a few MeV (Matteson 1982) and also the 0.5 MeV annihilation line (Lingenfelter and Ramaty 1982). These features could be due to a hot, two-temperature disk around a central black hole. We explore the energetic source at the galactic center more fully elsewhere (Kafatos and Eilek 1983).

##### b) Extragalactic Sources

Three active galactic nuclei have been seen so far in  $\gamma$ -rays. Kafatos (1980) summarizes these observations. The nucleus of Cen A has been seen out to 30 MeV (Hall *et al.* 1976) and is also detected at 300 GeV (Grindlay *et al.* 1975) with  $L(>1 \text{ MeV}) \sim 0.2 L_{\text{bol}}$ . The quasar 3C 273 has been seen out to 500 MeV (Swanenburg *et al.* 1978) with  $L(>1 \text{ MeV}) \sim 0.6 L_{\text{bol}}$ . NGC 4151 has been detected out to 100 MeV (Schonfelder 1978), with  $L(>1 \text{ MeV}) \sim 0.5 L_{\text{bol}}$ . All three spectra can be fitted by power laws with breaks (cf. Kafatos 1980). Except for the 300 GeV emission

from Cen A, which is too energetic to come from the basically thermal processes in our models, these data are not inconsistent with our models. However, there are hardly enough data here to test various theories.

Future observations of individual active objects will be useful. The relative luminosity above and below 100 keV, and any relation between the power law slope below 100 keV and the presence of 100 MeV emission, will be particularly good discriminants of the model. The Gamma Ray Observatory, in particular, is predicted to be sensitive to  $10^{-4}$  photons  $\text{cm}^{-2} \text{s}^{-1} \text{MeV}^{-1}$  at 0.5–1.0 MeV and to  $10^{-5}$  photons  $\text{cm}^{-2} \text{s}^{-1} \text{MeV}^{-1}$  at 1–10 MeV. These sensitivity levels translate to detectable luminosities of  $3 \times 10^{47} z^2 \text{ ergs s}^{-1}$  (0.5–1.0 MeV) and  $9 \times 10^{46} z^2 \text{ ergs s}^{-1}$  (1–10 MeV), if  $H_0 = 75 \text{ km s}^{-1} \text{ Mpc}^{-1}$ .

However, present day observations of quasars at lower X-ray energies sample many more objects and may provide insight to the applicability of these models. Mushotzky *et al.* (1980) observed several nearby active galactic nuclei from 2 to 50 keV and found the energy spectrum to be a power law with slope  $-0.7 \pm 0.1$ . (This would imply  $\gamma \approx 1$  in our picture.) Most of their objects are not radio strong. The *Einstein* X-Ray Observatory has detected 80% of the quasars it observed at 2 keV (Zamorani *et al.* 1981; Ku, Helfand, and Lucy 1980). It appears that radio-strong quasars have relatively higher X-ray luminosities (compared, for instance, to their optical luminosity) but that radio-weak objects are still X-ray sources.

If, indeed, a two-temperature accretion disk around a massive black hole exists in an active nucleus, the calculations in this paper suggest that the fractional mass accretion rate may be the important parameter in distinguishing radio-weak and radio-strong models. When  $\dot{M}/\dot{M}$  is low, the hot electrons in the disk still produce a power law X-ray spectrum out to  $\sim 100$  keV, as seen by Mushotzky *et al.* (1980). When  $\dot{M}/\dot{M}$  is larger, the high pion production provides a strong source of  $\gamma$ -rays (at a few MeV if the disk is optically thick) and also a strong source of relativistic particles. These particles could be the seeds of further acceleration and radiation processes; in particular they could produce the nonthermal synchrotron and self-Compton spectrum which seems to be seen in radio-strong quasars. (See Jones, O'Dell, and Stein 1974 for the synchrotron self-Compton model; and, recently, Owen, Helfand, and Spangler 1981 and Owen and Puschell 1982 for observations pertinent to the possible mixture of thermal and nonthermal components in quasar spectra.)

### c) The $\gamma$ -Ray Background

Finally, a powerful indirect measurement of the high-energy spectrum of active nuclei may come from the  $\gamma$ -ray background. Below  $\sim 50$  keV the background is well fitted by a thermal bremsstrahlung spectrum at  $kT_e = 40$  keV (cf. Boldt 1980). Above 50 keV, it appears to follow a power law, or several power laws with breaks; in particular, there is some evidence for a bump and steepening at a few MeV (Schonfelder, Grami, and Penningsfeld 1980), although this latter has been questioned (Setti and Woltjer 1982). There has been much discussion about the high-energy background being due to discrete sources, especially quasars (for instance, Bignami *et al.* 1979; Setti and Woltjer; and references therein). The power law below a few MeV, the apparent steepening at a few MeV, and the relatively small luminosity at very high energies, all provide strong constraints on the "average" quasar. Kafatos and Eilek (1982) find that the two-temperature accretion disk models of this paper with  $\gamma \sim 1-3$  and  $\dot{M} \sim 0.1-1$  of the Eddington limit may be a good model for the spectrum of this typical "background" quasar.

We wish to thank R. Mushotzky and P. Noerdlinger for illuminating discussions. J. E. is grateful for the hospitality of the 1980 Aspen Workshop on Astrophysics, where some of this work was carried out.

## APPENDIX

We follow Novikov and Thorne (1973) in writing down the basic structure equations for a Keplerian,  $\alpha$ -viscosity disk in a Kerr metric (which reduces to Schwarzschild if  $a_* = 0$ ). Novikov and Thorne give the analytic metric structure factors  $\mathcal{A}$ ,  $\mathcal{B}$ ,  $\mathcal{C}$ ,  $\mathcal{D}$ , and  $\mathcal{E}$ , and an integral representation of  $\mathcal{Q}$ ; Page and Thorne (1974) give an explicit form for  $\mathcal{Q}$  and one correction to the Novikov and Thorne factors. We refer the reader to these papers for the (rather long) formulae, and here we simply list the compound factors that appear in the structure equations:

$$f_1(r) = \mathcal{B}^2 \mathcal{D} \mathcal{E} / \mathcal{A}^2 \mathcal{C}, \quad f_2(r) = \mathcal{C} / 2\mathcal{Q} / \mathcal{B} \mathcal{D}, \quad f_3(r) = \mathcal{Q} / \mathcal{B} \mathcal{C}^{1/2}. \quad (\text{A1})$$

We emphasize that these are functions of radius. Paper I illustrates their behavior.

The structure equations for the disk are:

$$\text{vertical hydrostatic support:} \quad p = GM_p n h^2 f_1(r) / r^3; \quad (\text{A2})$$



$$\text{angular momentum transport: } 4\pi r^2 \alpha p h = r v_\phi(r) \dot{M} f_2(r); \quad (\text{A3})$$

$$\text{ion thermal balance: } \frac{3}{8\pi} \frac{GMM}{r^3 h} f_3(r) = 6 \times 10^{-3} m_p \ln \Lambda n^2 k \frac{(T_i - T_e)}{T_e^{3/2}} + \lambda_\pi(T_i) n^2; \quad (\text{A4})$$

$$\text{unsaturated Compton cooling: } 4kT_e = m_e c^2 y / g(\tau_{\text{cs}}). \quad (\text{A5})$$

Here,  $g(\tau_{\text{cs}}) = \max(\tau_{\text{cs}}, \tau_{\text{cs}}^2)$ ;  $\lambda_\pi(T_i) n^2$  is the ion energy loss per volume through pion processes; the other terms have their usual meaning. The function  $\lambda_\pi(T_i)$  can be found from the  $\langle \sigma v \rangle$  curve given by Dahlbacka, Chapline, and Weaver (1974). The fudge factors in (A3) and (A5) are  $\alpha$ , the viscosity parameter, which we take to be 0.1 and 1.0 in our models, and  $y$ , the Comptonization parameter, which we take as 0.3, 1.0, and 3.0. The system of equations is completed with the state equation,  $p = nk(T_i + T_e)$ , and the optical depth definition,  $\tau_{\text{cs}} = 6.65 \times 10^{-25} nh$ . This gives six equations in the unknown  $(T_i, T_e, n, p, h, \tau_{\text{cs}})$  which can be reduced to a single equation in  $\tau_{\text{cs}}$ ,

$$\begin{aligned} \frac{2.9 \times 10^{-2}}{\alpha y^{3/2}} \left( \frac{\dot{M}_\star}{M_8} \right) \left( \frac{f_2(r_\star)}{r_\star^{3/2}} \right) \tau_{\text{cs}}^3 g(\tau_{\text{cs}})^{3/2} - \frac{1.5 \times 10^{-6}}{y^{1/2}} \tau_{\text{cs}}^3 g(\tau_{\text{cs}})^{1/2} \\ + 2.2 \times 10^{15} \lambda_\pi(T_i) \tau_{\text{cs}}^{5/2} = \frac{1}{\alpha^{1/2}} \left( \frac{\dot{M}_\star}{M_8} \right) \frac{f_2(r_\star)^{1/2} f_3(r_\star)}{f_1(r_\star)^{1/2} r_\star^{9/4}}. \end{aligned} \quad (\text{A6})$$

We have parameterized  $M_8 = M/10^8 M_\odot$ ,  $\dot{M}_\star = M/1 M_\odot \text{ yr}^{-1}$  and  $r_\star = rc^2/GM = r/(1.5 \times 10^{13} M_8) \text{ cm}$ .

In general (A6) must be solved numerically for  $\tau_{\text{cs}}$ , and then the rest of the unknowns can be found directly. This was done in our numerical models. However, when  $T_i \gg T_e$  and when the pion cooling is small, the second and third terms in (A6) are small and an analytic solution for  $\tau_{\text{cs}}$  is possible. This is given in Table 2.

#### REFERENCES

- Bardeen, J. M., Press, W. H., and Teukolsky, S. A. 1972, *Ap. J.*, **178**, 347.  
 Bignami, G. F., Fichtel, C. W., Hartman, R. C., and Thompson, D. J. 1979, *Ap. J.*, **232**, 649.  
 Boldt, E. 1980, Invited lecture at 155th AAS meeting, San Francisco.  
 Caroff, L. J., Eilek, J. E., and Noerdlinger, P. N. 1983, in preparation.  
 Cavallo, G., and Rees, M. J. 1978, *M.N.R.A.S.*, **183**, 359.  
 Crannell, C. J., Joyce, G., and Ramaty, R. 1976, *Ap. J.*, **210**, 582.  
 Cunningham, C. T. 1975, *Ap. J.*, **202**, 738.  
 Dahlbacka, G. H., Chapline, G. F., and Weaver, T. A. 1974, *Nature*, **250**, 36.  
 Eardley, D. M., and Lightman, A. P. 1975, *Ap. J.*, **200**, 187.  
 Eardley, D. M., Lightman, A. P., Payne, D. G., and Shapiro, S. L. 1978, *Ap. J.*, **224**, 53.  
 Eilek, J. A. 1980, *Ap. J.*, **236**, 664 (Paper I).  
 Eilek, J. A., and Caroff, L. J., 1979, *Ap. J.*, **233**, 463.  
 Fazio, G. G. 1967, *Ann. Rev. Astr. Ap.*, **5**, 481.  
 Grindlay, J. E., Helmken, H. F., Hanbury Brown, R., David, J., and Allen, L. R. 1975, *Ap. J. (Letters)*, **197**, L9.  
 Hall, R. D., Meegan, C. A., Walraven, G. D., Djoth, F. T., and Haymes, R. C. 1976, *Ap. J.*, **210**, 631.  
 Helmken, H. F., and Weeks, T. 1978, San Diego X-ray and Gamma-Ray Astronomy Meeting.  
 Higdon, J. C., and Lingenfelter, R. E. 1977, *Ap. J. (Letters)*, **215**, L53.  
 Holt, S. S., and McCray, R. 1982, *Ann. Rev. Astr. Ap.*, **20**, 323.  
 Jones, F. C. 1963, *J. Geophys. Res.*, **68**, 4399.  
 Jones, T. W., O'Dell, S. L., and Stein, W. H. 1974, *Ap. J.*, **188**, 353.  
 Kafatos, M. 1980, *Ap. J.*, **236**, 99.  
 Kafatos, M., and Eilek, J. A. 1982, in *IAU Symposium 104*, to be published.  
 ———. 1983, in preparation.  
 Kafatos, M., and Leiter, D. 1979, *Ap. J.*, **229**, 46.  
 Ku, W. H., Helfand, D. J., and Lucy, L. B. 1980, *Nature*, **288**, 323.  
 Leiter, D., and Kafatos, M., 1978, *Ap. J.*, **226**, 32.  
 Liang, E. P. T. 1979, *Ap. J.*, **234**, 1105.  
 Liang, E. P. T., and Price, R. H. 1977, *Ap. J.*, **218**, 247.  
 Liang, E. P. T., and Thompson, K. A. 1979, *M.N.R.A.S.*, **189**, 421 (LT).  
 ———. 1980, *Ap. J.*, **240**, 271.  
 Lightman, A. P., and Eardley, D. M. 1974, *Ap. J. (Letters)*, **187**, L1.  
 Lingenfelter, R. E., and Ramaty, R. 1982, in *The Galactic Center*, ed. G. R. Riegler and R. D. Blandford (New York: Am. Inst. Phys.).  
 Lo, K. Y. 1982, in *The Galactic Center*, ed. G. R. Riegler and R. D. Blandford (New York: Am. Inst. Phys.).  
 Marscher, A. P., Vestrand, W. T., and Scott, J. S. 1980, *Ap. J.*, **241**, 1166.  
 Matteson, J. L. 1982, in *The Galactic Center*, ed. G. R. Riegler and R. D. Blandford (New York: Am. Inst. Phys.).  
 McBreen, B. 1979, *Astr. Ap.*, **71**, L21.  
 Mushotzky, R., Marshall, F., Boldt, E., Holt, S., and Serlemitsos, P. 1980, *Ap. J.*, **235**, 377.  
 Nolan, P. L., Gruber, D. E., Knight, F. K., Matteson, J. L., Rothschild, R. E., Marshall, F. E., Levine, A. M. and Primini, F. A. 1981, *Nature*, **293**, 275.  
 Novikov, I. D., and Thorne, K. S. 1973, in *Black Holes*, ed. C. DeWitt and B. S. Dewitt, (New York: Gordon & Breach).  
 Owen, F. N., Helfand, D. J., and Spangler, S. R. 1981, *Ap. J. (Letters)*, **250**, L55.  
 Owen, F. N., and Puschell, J. J. 1982, *Ap. J.*, **87**, 595.  
 Page, D. N., and Thorne, K. S. 1974, *Ap. J.*, **191**, 499.  
 Perola, G. C., Scarsi, L., and Sironi, G. 1967, *Nuovo Cimento*, **52B**, 455.  
 Piran, T. 1978, *Ap. J.*, **221**, 652.  
 Piran, T., and Shaham, J. 1977, *Phys. Rev. D*, **16**, 1615.  
 Pringle, J. E. 1976, *M.N.R.A.S.*, **177**, 65.

- Pringle, J. E., Rees, M. J., and Pacholczyk, A. G. 1973, *Astr. Ap.*, **29**, 179.
- Ramaty, R., and Lingenfelter, R. E. 1966, *J. Geophys. Res.*, **71**, 3687.
- Rybicki, G. B., and Lightman, A. P. 1979, *Radiative Processes in Astrophysics* (New York: Wiley Interscience).
- Schonfelder, V. 1978, *Nature*, **274**, 344.
- Schonfelder, V., Grami, F., and Penningsfeld, F. P. 1980, *Ap. J.*, **240**, 350.
- Setti, F., and Woltjer, L. 1981, in *Cosmology and Fundamental Physics* (Rome: Proc. Vatican Study Week).
- Shapiro, S. L., Lightman, A. P., and Eardley, D. M. 1976, *Ap. J.*, **204**, 187 (SLE).
- Stecker, F. W. 1973, *Ap. J.*, **185**, 499.
- Stoeger, W. J. 1980, preprint.
- Swanenburg, B. N., *et al.* 1978, *Nature*, **275**, 298.
- Synge, J. L. 1957, *The Relativistic Gas* (Amsterdam: North-Holland).
- Thorne, K. S. 1974, *Ap.*, **191**, 507.
- Zamorani, G., 1981, *Ap. J.*, **245**, 357.

JEAN A. EILEK: Physics Department, New Mexico Tech, Socorro, NM 87801

MINAS KAFATOS: Physics Department, George Mason University, 4400 University Drive, Fairfax, VA 22030